Engagement of CD99 Activates Distinct Programs in Ewing Sarcoma and Macrophages

Maria Cristina Manara[1], Cristina Manferdini[2], Camilla Cristalli[1], Marianna Carrabotta[1], Spartaco Santi[3,4], Alessandra De Feo[1], Giulia Caldoni[1], Michela Pasello[1], Lorena Landuzzi[1], Pier-Luigi Lollini[5], Francesca Salamanna[6], Sabrina Dominici[7], Valentina Fiori[7], Mauro Magnani[8], Gina Lisignoli[2], and Katia Scotlandi[1]

ABSTRACT

Ewing sarcoma (EWS) is the second most common pediatric bone tumor. The EWS tumor microenvironment is largely recognized as immune-cold, with macrophages being the most abundant immune cells and their presence associated with worse patient prognosis. Expression of CD99 is a hallmark of EWS cells, and its targeting induces inhibition of EWS tumor growth through a poorly understood mechanism. In this study, we analyzed CD99 expression and functions on macrophages and investigated whether the concomitant targeting of CD99 on both tumor and macrophages could explain the inhibitory effect of this approach against EWS. Targeting CD99 on EWS cells downregulated expression of the "don't eat-me" CD47 molecule but increased levels of the "eat-me" phosphatidyl serine and calreticulin molecules on the outer leaflet of the tumor cell membrane, triggering phagocytosis and digestion of EWS cells by macrophages. In addition, CD99 ligation induced reprogramming of undifferentiated M0 macrophages and M2-like macrophages toward the inflammatory M1-like phenotype. These events resulted in the inhibition of EWS tumor growth. Thus, this study reveals what we believe to be a previously unrecognized function of CD99, which engenders a virtuous circle that delivers intrinsic cell death signals to EWS cells, favors tumor cell phagocytosis by macrophages, and promotes the expression of various molecules and cytokines, which are pro-inflammatory and usually associated with tumor regression. This raises the possibility that CD99 may be involved in boosting the antitumor activity of macrophages.

Introduction

Treating patients with Ewing sarcoma (EWS), the second most frequent pediatric tumor of the bone, remains a challenge for oncologists because of the paucity of novel effective drugs for patients who do not respond to first-line chemotherapy and for patients with metastatic disease. In an effort to identify novel therapeutic strategies, we have studied the relevance of CD99, a glycosylated transmembrane protein that has gained research interest because of its involvement in many essential cellular functions, such as cell adhesion and migration, cell death and differentiation, intracellular protein trafficking, endocytosis, and exocytosis of immune and tumor cells (1). CD99 is expressed at high levels in EWS cells and cooperates with the oncogenic driver EWSR1::FLI1 (2) to maintain EWS malignancy (3, 4), thereby emerging as a promising therapeutic target (5). Engagement of CD99 with antibodies (Abs), including the human diabody (dAbd) C7 (6), has been shown to deliver potent lethal signals in EWS cells independent of the canonical apoptosis pathway (7–9), leading to synergistic effects with conventional chemotherapeutic agents when mice bearing EWS are treated with a combination of anti-CD99 and doxorubicin or irinotecan (8, 10, 11).

In addition to its effects on EWS tumor cells, CD99 has been implicated in the regulation of several immune cell functions, such as proliferation and stimulation of mature peripheral T cells, regulation of MHC class I molecule transport from the Golgi complex to the cell surface, T-cell migration, and diapedesis of monocytes across the endothelium (1). Moreover, CD99 is an important player in lymphocyte development. CD99-deficient fetuses typically demonstrate a marked impairment in thymic development, suggesting a role for CD99 in normal thymus ontogeny (12). In thymocytes, CD99 elicits homotypic cell aggregation and induces cell death at critical stages of thymocyte differentiation (13–15). Ligation of CD99 by Abs induces a death pathway named "death by neglect" in $CD4^+CD8^+$ double-positive thymocytes that do not recognize peptide-loaded self-MHC molecules present in the thymus (16).

In both EWS cells and immature thymocytes, CD99 engagement induces phosphatidylserine (PS) exposure on the cell surface (17–19), but cell death proceeds through classical or nonclassical apoptotic pathways, depending on the different CD99 domains that are activated by distinct Abs (6, 15, 17). The reason(s) why different CD99 domains are linked to different death pathways is not clear, but the induction of cell death independent of canonical apoptosis may be an opportunity to treat EWS patients resistant to canonical apoptosis–inducing agents (20).

[1]Laboratory of Experimental Oncology, IRCCS Istituto Ortopedico Rizzoli, Bologna, Italy. [2]Laboratorio di Immunoreumatologia e Rigenerazione Tissutale, IRCCS Istituto Ortopedico Rizzoli, Bologna, Italy. [3]CNR Institute of Molecular Genetics "Luigi Luca Cavalli-Sforza", Unit of Bologna, Bologna, Italy. [4]IRCCS Istituto Ortopedico Rizzoli, Bologna, Italy. [5]Laboratory of Immunology and Biology of Metastasis, Department of Medical and Surgical Sciences (DIMEC), University of Bologna, Bologna, Italy. [6]Surgical Sciences and Technologies, IRCCS Istituto Ortopedico Rizzoli, Bologna, Italy. [7]Diatheva Srl, Cartoceto, Italy. [8]Department of Biomolecular Sciences, University of Urbino "Carlo Bo", Urbino, Italy.

M.C. Manara, C. Manferdini, and C. Cristalli contributed equally to this article.

Corresponding Authors: Katia Scotlandi, Laboratory of Experimental Oncology, IRCCS Istituto Ortopedico Rizzoli, via di Barbiano, 1/10, Bologna 40136, Italy. E-mail: katia.scotlandi@ior.it; and Gina Lisignoli, Laboratorio di Immunoreumatologia e Rigenerazione Tissutale, IRCCS Istituto Ortopedico Rizzoli, via di Barbiano, 1/10, Bologna 40136, Italy. E-mail: gina.lisignoli@ior.it

Cancer Immunol Res 2024;XX:XX–XX

doi: 10.1158/2326-6066.CIR-23-0440

In the thymus, apoptotic thymocytes are cleared by surrounding F4/80$^+$ macrophages (21), which, in response to the engulfment of apoptotic cells, release various molecules and cytokines that are known to promote thymocyte death (22–24). Because macrophages continually engulf apoptotic cells, they may constantly provide these cells with death-inducing signals and thus contribute to ensuring the effective induction of "death by neglect" in the thymus. In this study, we tested whether macrophages potentiate the CD99-induced death of EWS cells. Immune checkpoint–targeted therapies have yielded disappointing results in EWS (25, 26), likely due to the paucity of effector T cells (27, 28) in the EWS tumor microenvironment (TME). In contrast, macrophages, predominantly immunosuppressive M2-like macrophages, have been described as the most abundant cells in the EWS TME (27–29), and a high infiltration of M2-like macrophages in EWS samples is reported to be associated with a poor survival rate (30). Thus, EWS might benefit from the development of strategies focusing on macrophage activation/polarization rather than T cell–checkpoint modulation. CD99, besides being expressed on EWS cells is also present on monocytes/macrophages (31).

Here, we show that CD99 antibodies promote tumor growth inhibition through a dual action on tumor cells and macrophages: ligation of CD99 in EWS cells influences the redistribution of eat-me and don't-eat-me signals on EWS cell membranes, leading to enhanced phagocytic capabilities of macrophages and decreased tumor cell survival; and triggering of CD99 on M0/M2-like macrophages favors macrophage polarization toward an inflammatory M1-like phenotype (20).

Materials and Methods

In vitro cell cultures

We used the following human patient-derived EWS cell lines: TC-71 (DSMZ, Catalog no. ACC-516, RRID: CVCL_2213) and 6647 (RRID: CVCL_H722) both kindly provided by T. J. Triche (Children's Hospital, Los Angeles, CA); H-825 kindly provided by Prof. A. Llombart-Bosch (University of Valencia, Spain); and A673 cells (RRID: CVCL_0080) kindly provided by H. Kovar (St. Anna Kinderkrebsforschung). SK-N-MC (RRID: CVCL_0530), SK-ES-1 (RRID:CVCL_0627), and RD-ES (RRID:CVCL_2169) were purchased from the ATCC (Rockville, MD); LAP-35 (RRID:CVCL_A096) and IOR/CAR were established in our laboratory and have been previously characterized (8). The TC-EGFP cell line was derived from TC-71 cells transfected with the pEGFP-N1 plasmid (RRID: Addgene_172284, Clontech) to stably express Enhanced Green Fluorescent Protein (EGFP; ref. 32). Cells with silenced CD99 (TC-CD99-shRNA#1 and TC-CD99-shRNA#2) were also used (3). To avoid cross-contamination between cell lines and outgrowth of faster-growing clones in long-term cultures, all cell lines were kept in liquid nitrogen until use. When in culture, they were maintained in Iscove's modified Dulbecco's medium (IMDM, EuroClone, #ECB2072L) supplemented with 10% FBS (EuroClone, #ECS0180L) and incubated at 37°C in a humidified atmosphere containing 5% CO_2 for approximately 8–12 *in vitro* passages (corresponding to 2–3 months) before being discarded. Whenever necessary, replicates started from the same batch of frozen vials. Cells were regularly tested for *Mycoplasma* contamination (MycoAlert Mycoplasma Detection Kit, LT07–418, Lonza) and authenticated by short tandem repeat PCR analysis using a PowerPlex ESX Fast System kit (CLA service by Eurofins Genomics; before starting the experiments and at the end (last control July 2023). Human Bone marrow mesenchymal stem cells (hBM-MSCs) were purchased from Lonza (Catalog no. 2M-302) and used within 8 *in vitro* passages.

Ethics

The study was approved by the Ethical Committee of the Rizzoli Orthopedic Institute and Comitato Etico di Area Vasta Emilia Centro (Prot. 0019012 del 15/09/2016 and CE-AVEC:505/2019/Sper/IOR). Informed consent for human peripheral blood mononuclear cells (PBMC) collection was obtained from all healthy donors, with participants signing a printed consent form (Prot. N° 1212 del 15.1.2015). Informed consent for patient-derived xenograft (PDX) collection was obtained signing a printed consent form (Prot. 000923 2016/04/22). All animal procedures were performed in accordance with ARRIVE guidelines (33) and with European directive 2010/63/UE and Italian Law (DL 26/2014); experimental protocols were reviewed and approved by the institutional animal care and use committee ("Comitato per il Benessere Animale") of the University of Bologna and by the Italian Ministry of Health with letters 4783-X/10 and 208/2017-PR and 1051/2020-PR as previously reported (8, 11).

In vivo studies

Female athymic 4- to 5-week-old Crl:CD-1nu/nuBR mice (Charles River Italia) were subcutaneously injected with 5×10^6 6647 cells. Starting from day +7 after cell injection, when tumors reached a volume of approximately 10 mm^3, that is, a mean diameter of 2.7 mm at least, the animals were randomized into two groups: control group, mice that received subcutaneous injections of PBS or vehicle; and dAbd C7-treated group, mice received daily subcutaneous peritumoral injections of the anti-CD99 human monospecific bivalent single-chain fragment variable dAbd C7 produced by Diatheva Srl (1 mg/injection) for two subsequent cycles of 5 days, as previously reported (8).

For studies using PDXs, immunodeficient NOD/SCID gamma (NSG; Charles River Italia) male mice 6- to 11-week-old or 8- to 25-week-old immunodeficient BALB/c Rag2−/−; Il2rg−/− (RGKO) were implanted subcutaneously in the interscapular region with fragments of PDX-EW#2 or PDX-EW#3, which we previously developed in our lab (11). RGKO mice were bred in our animal facilities from founders kindly given to us by Drs. T. Nomura and M. Ito of the Central Institute for Experimental Animals (Kawasaki, Japan; ref. 34). Pharmacologic treatments started 3 weeks after tumor fragment implantation, when tumors reached a volume of at least 10 mm^3. For peritumoral administration of dAbd C7, animals were randomized to receive two cycles of dAbd C7 (1 mg/injection, 5 days/week for 2 consecutive weeks followed by 1 week of rest). Control mice were not treated, as previously reported (11). For systemic administration of dAbd C7, animals were randomized to receive two cycles of dAbd C7 (50 mg/Kg) by intraperitoneal injection 5 days/week for 2 consecutive weeks followed by 1 week of rest (35). Control mice were not treated. Tumor size was measured with calipers, and tumor volumes were calculated according to the formula $\pi/2\ [\sqrt{(a \times b)}]^3/6$, where a = maximal tumor diameter and b = tumor diameter perpendicular to a. Mouse body weight and tumor volume were measured at least once a week. The experimental humane endpoint was a maximum tumor volume of 2.5 cm^3 and all mice were sacrificed as soon as an experimental group (usually untreated controls) overcame this threshold. At necropsy, the tumors were collected and stored for histopathologic and molecular analyses to evaluate the effects of dAbd C7 treatment on the immune phenotype of tumor cells and tumor immune microenvironment.

Human blood samples processing and macrophages preparation

PBMCs from healthy human volunteers were isolated using density gradient Histopaque-1077 (#10771, Sigma-Aldrich) or purchased from Lonza (hPBMCs Lonza CC-2702 19TL064725). Monocytes were isolated by positive magnetic separation using CD14 immunomagnetic beads (#130–050–201 Miltenyi Biotec GmbH), followed by MACS LS column separation (#130–042–401 Miltenyi), according to the manufacturer's recommendations.

1×10^5 $CD14^+$ monocytes were plated in 60 mm petri dishes, maintained in IMDM (#ECB2072L, EuroClone) supplemented with 10% FBS (#ECS0180L, EuroClone), 100 U/mL penicillin, and 100 mg/mL streptomycin (#P0781–100, Merck), and incubated at 37°C in 5% CO_2 for 7 days to obtain M0-like macrophages. To obtain M1- and M2-like macrophages, $CD14^+$ monocytes were cultured as for M0-like macrophages with the addition of 50 ng/mL recombinant human GM-CSF (#130–093–865, Miltenyi) or 10 ng/mL M-CSF (#130–096–491, Miltenyi), respectively. Subsequent activation was achieved through stimulation for a further 48 hours with 10 ng/mL recombinant human IFNγ (#285IF, R&D Systems) or 10 ng/mL IL4 (#204-IL; R&D Systems), respectively (36). Before starting the experiments, M0-, M1-, and M2-like macrophages were phenotypically characterized by flow cytometry (see *Flow cytometry*) and cytokines were analyzed on cells starved for 48 hours (see *Multiplex cytokine assay* and *qRT-PCR analysis*), to remove stimulating factors.

Mouse peritoneal lavage

Peritoneal lavages were carried out on naïve NSG mice after sacrifice, by injecting 5 mL of PBS into the peritoneal cavity (37). After gentle massage, the peritoneal fluid was collected and put into a conical tube on ice. To reduce nonspecific binding of antibodies, Fc receptors were blocked by incubation with anti-CD16/CD32 Fc-block (# 553142, BD Biosciences, RRID:AB_394657) before staining with PE/Cy7-conjugated anti-mouse F4/80 (clone MB8) (#123114, BioLegend, RRID:AB_893478), which was used as a marker of peritoneal macrophages, or double staining with PE/Cy7-conjugated anti-mouse F4/80 and anti-human CD99 dAbd C7 (Diatheva Srl) followed by incubation with FITC-conjugated Protein A (#BA1120–0.5, Boster-Bio). Levels of expression were analyzed by flow cytometry (see *Flow cytometry*).

In vitro anti-CD99 treatments

EWS cells or macrophages were treated with mAb 0662 (10 μg/mL), mAb 12E7 (10 μg/mL), or dAbd C7 (200 μg/mL) for 5 minutes to 6 hours before processing as described below. The hybridoma used to produce murine anti-CD99 mAb 0662 was kindly provided by Alain Bernard (Unité INSERM 343, Hospital de l'Archet, Nice). The mAb 12E7 was purchased from Santa Cruz Biotechnology (sc-53148, Santa Cruz, mouse monoclonal, RRID: AB_629249). An irrelevant antibody (MOPC-21, #M7894, Sigma-Aldrich, RRID: AB_1163632) (10 μg/mL) was used as an additional control.

For the coculture assay, 5×10^5 EWS cells treated or untreated with anti-CD99 were seeded on M0 or M2-like macrophages. After 6 hours, macrophages were extensively washed to remove tumor cells and further analyzed by phagocytosis assay and quantitative real-time PCR (qRT-PCR). Cell supernatants were also collected and analyzed by multiplex cytokine assay. Alternatively, 1×10^5 macrophages treated or untreated with anti-CD99 were cocultured with 5×10^5 untreated EWS cells. After 6 hours, macrophages were extensively washed to remove tumor cells and further analyzed by phagocytosis assay and qRT-PCR. Cell supernatants were also collected and analyzed by multiplex cytokine assay. Cytotoxicity against EWS cells elicited by macrophages was measured by vital cell counting using Trypan Blue dye exclusion (#T8154, Sigma). At least three separate experiments were performed using macrophages for each analysis.

Recombinant human and mouse CD99 extracellular domain production

The recombinant extracellular domain of human CD99 (aa 23–123) was produced using the plasmid pQE30a–CD99/His in TG1 *E. coli* cells (38). The plasmid containing the full-length mouse CD99 cDNA (GenBank: BC019482.1) was a kind gift from prof. Mario Paolo Colombo (Fondazione IRCCS Istituto Nazionale dei Tumori, Experimental Oncology Department, Molecular Immunology Unit, Milan). This plasmid was used as template for the PCR amplification of the extracellular domain of mouse CD99 corresponding to aa 29–138 with the primers: mmCD99BamHI Fw: 5′-GGCGCGGATCCTGACG ACTTCAACCT-3′ and mmCD99XhoI Rev: 5′-ACCACCTCGAGC-TACAAGCCCTGGGGCGT-3′. Amplified fragment, was agarose-purified using the Gel MiniElute Extraction kit (#28604, Qiagen) and digested, together with the plasmid pET45b(+) (#71327–3, Novagen), with the restriction enzymes XhoI and BamHI (#R0146S and #R0136S, respectively, New England Biolabs) at 37°C for 3 hours. Digested insert and vector were ligated with T4 DNA ligase (#M1801, Promega) for 16 hours at +4°C. The final construct contains a His tag at the N-terminal of the CD99 extracellular domain. Ligation mixes were transformed into the *Escherichia coli* (Ec) strain BL21 (DE3) [(F-ompT hsdSB(rB-mB-) gal dcm (DE3)] for protein expression. Positive clones were screened by colony-PCR and the sequence confirmed by sequencing. Recombinant human and mouse CD99 extracellular domains were produced in Ec using the protocol described in (39).

CD99 ELISA

2HB 96-well plates were coated with 100 μL/well of rCD99 antigens diluted at 5 μg/mL in carbonate buffer pH 9.6 and kept at 37°C for 16 to 18 hours. After five washes in PBS containing Tween-20 0.05%, the plates were blocked with BSA (#A4503, Sigma) 1% in PBS (150 μL/well) and kept for 1 hour at 37°C. After washing, serial dilutions of dAbd C7 (Diatheva Srl) in PBS-BSA were added to the wells and the plates incubated for 90 minutes at 37°C. After washing, an anti-scFv polyclonal antibody (Diatheva Srl) was added and kept for 1 hour at 37°C. The immunoreactive signals were highlighted after further addition of a goat anti-rabbit HRP-conjugated antibody (#1706515, Bio-Rad, RRID: AB11125142). After incubation and washing, the substrate ABTS (#11684302001, Roche Diagnostic) was added, and the absorbance values were obtained reading at 405 nm with a microplate reader (Glomax Multi Detection System).

In vitro phagocytosis assays

To evaluate phagocytic ability, human macrophages obtained as described in *human blood samples processing and macrophages preparation* were treated and cocultured with TC-EGFP cells as described above (*In vitro anti-CD99 treatments*), repeatedly washed with PBS, fixed in 4% paraformaldehyde for 10 minutes at room temperature, and subsequently imaged with a fluorescence microscope Nikon 90i Eclipse with a 20x NA 0.5 Refractive Index: 1 Plan Apo objective. Images of 1280 × 960 pixels were collected using a Nikon DS-U2/L2 USB digital camera. Transmission and fluorescence images were merged and rendered using NIS Elements software (Nikon). The phagocytic index was calculated as the number of phagocytosed EWS

cells per at least 100 macrophages and was expressed as a percentage (%) of macrophages with engulfed cells.

Time-lapse confocal imaging

Confocal fluorescence images related to phagocytosis assays were acquired using a Nikon A1R confocal microscope with a 20x NA 0.75 Plan Apo VC objective. All experiments were carried out at 37°C and 5% CO_2 using a stage incubation (OkoLab, Italy) and an Eclipse Ti-E inverted microscope equipped with a perfect focus system. 489.1 nm diode laser was used for excitation of GFP and was set at 12% to minimize the possible phototoxic effects induced by fluorescence illumination on live cells. The fluorescence emission was measured at 525/50 nm using a PMT detector. The diameter of the detection pinhole was set at two Airy units (59 μm) to generate a single thick optical section passing through the center of the cells. A series of sequential images of 1024 × 1024 pixels at 12-bits (4096 Gy levels) were collected at a fixed pixel size of 62 μm every 300 s for at least 10 hours. The transmission and fluorescence images were merged and rendered using NIS Elements Advanced Research software.

IHC

Serial 4-μm-thick paraffin sections from formalin-fixed, paraffin-embedded xenografts, obtained as described above (see *In vivo studies*) and as previously reported (8, 11), were processed according to standardized IHC procedures and then immunostained with the following antibodies: anti-CD47 (clone EPR21794; #ab218810, rabbit monoclonal, Abcam), anti-F4/80, (D2S9R) (#70076, rabbit polyclonal, Cell Signaling, RRID: AB_2799771), anti-CD206 (#ab64693, rabbit polyclonal, Abcam, RRID: AB_1523910), and anti-CD99 (O13) (#915601; BioLegend, RRID:AB_2565169). An avidin–biotin–HRP method was used for single staining (VECTASTAIN ABC kit, PK-4001, Vector Laboratories). A polymer with anti-mouse alkaline phosphatase and anti-rabbit HRP was used for dual staining (Mach2 Double Stain #1, #PBC-MRCT523L, Biocare Medical). For morphologic analyses, the slides were stained with hematoxylin and eosin.

Histologic and histomorphometric analyses were carried out with a digital pathology slide scanner with a resolution of 0.5 μm/pixel (Aperio AT2, Aperio Technologies, Vista, CA) using ImageScope software (v12.4.3, RRID: SCR_014311) for slide viewing and analysis.

qRT-PCR analysis

Total RNA from M0, M1, or M2-like macrophages cultured under different conditions (see *in vitro anti-CD99 treatment*) was extracted using RNA PURE reagent (#EMR506100, Euroclone Spa) according to the manufacturer's instructions and then treated with DNase I (#AM1906, DNA-free Kit, Life Technologies). Reverse transcription was performed using SuperScript VILO (#11754, Life Technology) reverse transcriptase and random hexamers according to the manufacturer's protocol. The forward and reverse primers for PCR amplification of the human genes encoding *CD80*, *CD86*, *CD163*, *CD206*, *IL1β*, *IL6*, *IL10*, and *TNFα* are described in Supplementary Table S1. RT-PCR was performed as previously described (40). The expression levels of target genes (RQ) were normalized to that of *GAPDH* and expressed as: $2^{-\Delta\Delta Ct}$, where ΔCt = Ct target genes – Ct GAPDH and $\Delta\Delta Ct = \Delta Ct$ sample − ΔCt calibrator (untreated cells at each time point).

Multiplex cytokine assay

The concentrations of IL1β, IL4, IL6, IL10, IL12, CCL4, CCL18, TNFα, and TGFβ were detected using multiplex bead-based sandwich immunoassay kits (Bio-Rad Laboratories Inc., #M500KCAF0Y, RRID: AB_2893118) following the manufacturer's instructions. Briefly, we added 50 μL to each well of the diluted standards (4-fold dilution series), controls, and samples in duplicate and add 50 μL of coupled beads, and the plates were incubated at room temperature for 30 minutes. The plates were then washed three time with 100 μL of wash buffer and incubated with 25 μL of detection antibodies for 30 minutes. Finally, the plates were washed three times, incubated with 50 μL of streptavidin-PE for 30 minutes, and measured in a Luminex Bio-plex system (Bio-Rad Laboratories Inc.). Data are expressed as pg/mL or as fold increase *versus* the control.

Flow cytometry

EWS cell lines, human macrophages (M0, M1, and M2-like) and hBM-MSCs were analyzed by flow cytometry (FACSCanto II cytometer; Becton Dickinson) using the following antibodies: anti-CD99-FITC (3B2/TA8)(# 11–0997–42, eBioscience, RRID:AB_2016685), anti-CD14-FITC (#F0844, Dako), anti-CD68-FITC (#562117, BD Pharmingen), anti-CD80-PE (#5572227, BD), anti-CD86-FITC (#374204, BioLegend), anti-CD163-PE/Cy7(#25–1639–4, Affymetrix), anti-CD206-APC (#561763, BD), anti-CD47-PE (REA 220) (#130–123–754, Miltenyi Biotech, RRID:AB_2819520), and anti-calreticulin-PE (EPR3924) (LSC105731, LSBio-Life Span, RRID: AB_2069806). Detection and quantification of PS-positive cells was performed by flow cytometric analysis of annexin-V-FITC/PI-labeled cells (MEBCYTO Apoptosis Kit #4700, Medical & Biological Laboratories). Data are expressed as % positive cells or median fluorescence intensity (MFI). Flow samples were properly analyzed using FCS Express 7.18.0025 software (RRID:SCR_016431).

Western blotting and immunoprecipitation

2×10^6 EWS cells (6647 and TC-71) were pretreated for 3 hours with MG132 10 μmol/L (Sigma, #C2211) and then exposed to 0662 (3 μg/mL) or dAbd C7 (200 μg/mL) for further 1 to 3 hours before being lysed with RIPA buffer (Thermo Fisher Scientific, #89900) containing protease inhibitors (Thermo Fisher Scientific, #A32955) and phosphatase inhibitors (Thermo Fisher Scientific, #A32957). 10×10^6 human macrophages obtained as described in *Human blood samples processing and macrophages preparation* and treated according to *In vitro anti-CD99 treatments section*. Western blotting was performed as previously described (8). Membranes were incubated overnight with the following primary antibodies: anti-Phospho-Stat1 (Tyr701) (D4A7) (#7649, rabbit monoclonal, RRID: AB_10950970), anti-c-Fos (9F6) (#2250, rabbit monoclonal RRID: AB_2247211), anti-c-Jun (60A8) (#9165, rabbit monoclonal, RRID: AB_2130165), anti-beta-Tubulin (SAP.4G5) (#T7816, mouse monoclonal RRID: AB_261770), and anti-GAPDH (14C10) (#2118, rabbit monoclonal, RRID: AB_561053) purchased from Cell Signaling Technology; and anti-Stat1 (#06–501, rabbit polyclonal, Millipore, RRID: AB_310145) and anti-CD47 (#ab218810, rabbit monoclonal, Abcam). Anti-rabbit IgG, Whole Ab ECL Antibody, HRP Conjugated (NA934, GeHealthcare, RRID: AB_772206) and Anti-mouse IgG, HRP Conjugated (NA9310, GeHealthcare, RRID: AB_772193) were used as the secondary antibodies and revealed by SuperSignal West Pico PLUS Chemiluminescent Substrate (#34580, Thermo Fisher Scientific).

For immunoprecipitation, 500 μg of cell lysates (as described above) obtained from 5×10^6 EWS cells (6647, TC-71 and TC-CD99-shRNA#2) were incubated for 16 hours with Protein G-Plus agarose beads (#sc-2003, Santa Cruz Biotechnology) in the presence of 2 μg anti-CD99 12E7 mAb (sc-53148, Santa Cruz, mouse monoclonal, RRID: AB_629249), anti-CD47 (#ab218810, rabbit monoclonal Abcam), or control IgG antibody (MOPC-21,

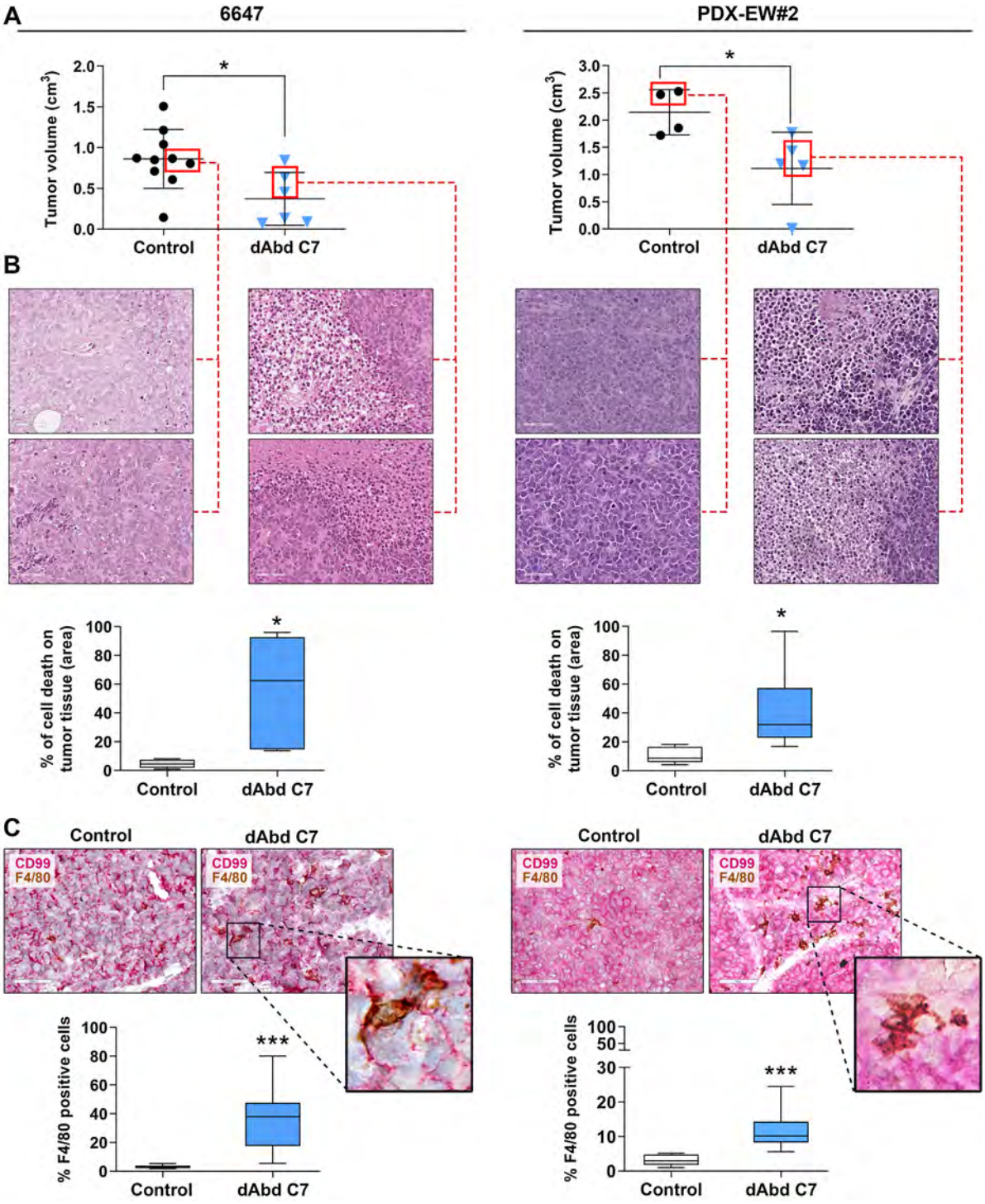

Figure 1.

The human anti-CD99 dAbd C7 inhibits tumor growth and increases macrophages infiltration. **A,** Tumor volume after treatment with the anti-CD99 dAbd C7 in xenografts derived from injection of 6647 cells in nude mice. Control, $n = 10$; dAbd C7, $n = 6$ (left) or PDX-EW#2 tumors developed in NSG mice; control, $n = 4$; dAbd C7, $n = 5$ (right). Dots represent single tumor volumes, mean ± SD are displayed. Mann–Whitney U test, *, $P < 0.05$. **B,** Representative H&E images of 6647 (left) or PDX-EW#2 (right) xenografts treated or not with dAbd C7 (scale bar, 50 μm). The tumor regions with nuclear condensation and the total area of the samples were identified by manually marking with Image J software. Histogram represents the percentage of tumor area with nuclear condensation (vs. total tumor area). Data are expressed as the median and range (minimum–maximum). Mann–Whitney U test, *, $P < 0.05$. **C,** Representative images of double staining IHC for F4/80 murine macrophages (brown) and CD99 EWS cells (red) in 6647 (left) or PDX-EW#2 (right) xenografts after treatment with dAbd C7 (scale bar, 50 μm). The enlarged box shows a mouse macrophage with engulfed EWS cells; the histograms represent the percentage of F4/80-positive cells calculated after evaluation of at least ten fields. Data are expressed as the median and range (minimum–maximum. Mann–Whitney U test; ***, $P < 0.001$.

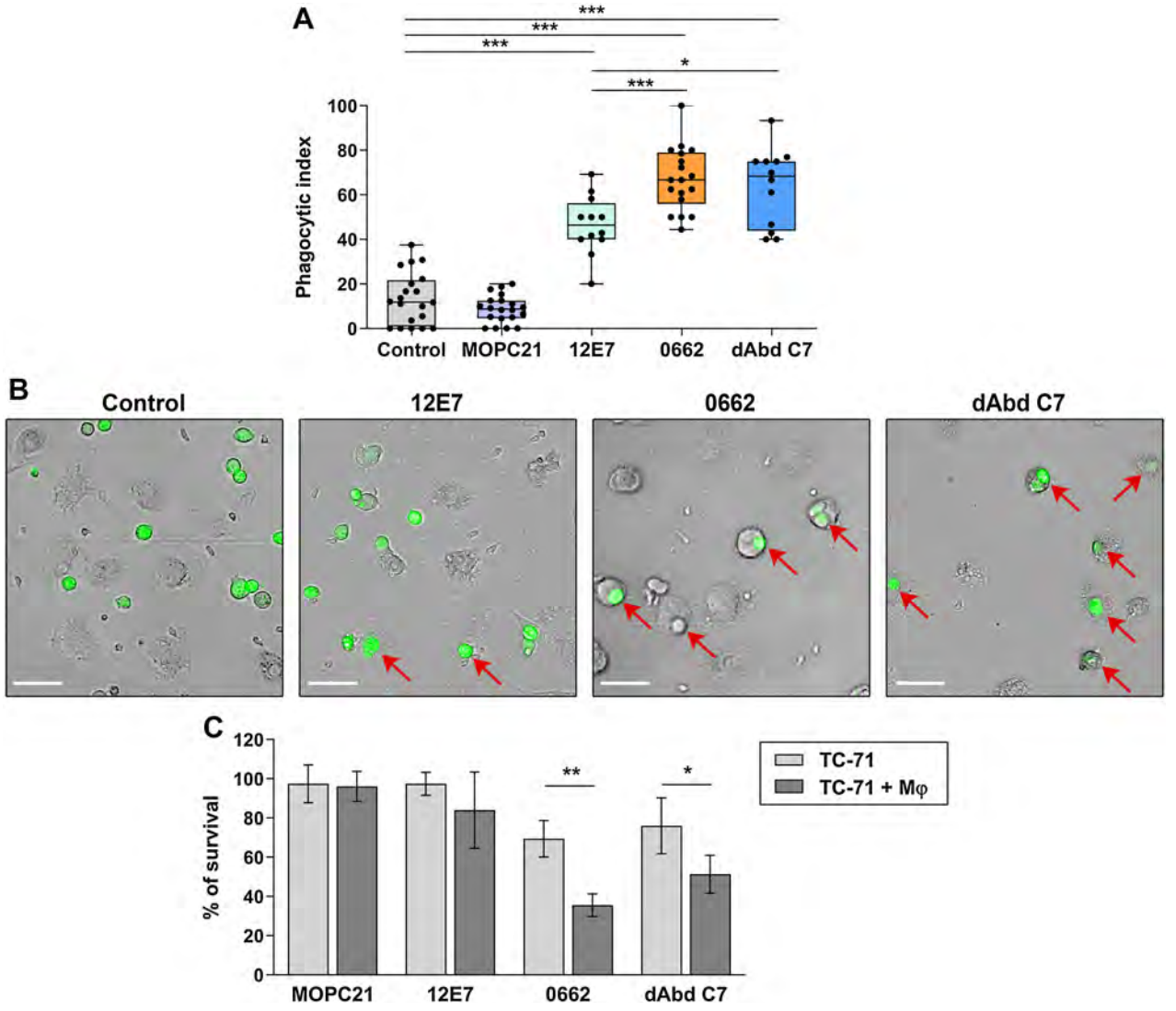

Figure 2.

Macrophage-mediated phagocytosis and cytotoxicity of EWS cells after anti-CD99 antibodies treatment. **A,** Phagocytic index of M0-like macrophages cocultured for 6 hours with TC-EGFP cells being exposed to anti-CD99 antibodies (12E7 mAb; 0662 mAb; dAbd C7 or to irrelevant MOPC21 antibody used as isotype control) for 30 minutes. Phagocytic index indicated the number of EWS cells phagocytosed per 100 macrophages. Dots represent single fields and data are expressed as the median and range (minimum–maximum) of at least three independent experiments. One-way ANOVA: *, $P < 0.05$; **, $P < 0.01$; ***, $P < 0.001$. **B,** Representative images of M0-like macrophages phagocytosing EWS cells after treatment with anti-CD99 antibodies. Arrows point to phagocytosed tumor cells (scale bar, 50 μm). **C,** EWS cell survival in the presence or not of M0-like macrophages (Mφ) detected by Trypan blue vital counting. Data are expressed as percentage compared with untreated TC-71 cells. Bars represent the mean ± SD of at least three independent experiments. Mann–Whitney U test: *, $P < 0.05$; **, $P < 0.01$.

#M7894, Sigma-Aldrich, RRID: AB_1163632). Immunoprecipitates and 20 μg of total lysates were then resolved on a 10% Tris-HCl gel and immunoblotted with anti-CD99 12E7 mAb (sc-53148, Santa Cruz, mouse monoclonal, RRID: AB_629249) and anti-CD47 mAb. Secondary anti-mouse and anti-rabbit antibodies were used and revealed as described earlier.

Statistics and reproducibility

Statistical analysis was performed using parametric tests for data with normal and symmetric distributions (one-way ANOVA, two-way ANOVA, and Tukey multiple comparison tests); otherwise, nonparametric tests were applied (Kruskal–Wallis and Dunn *post hoc* tests for unpaired data and Mann–Whitney U test for unpaired two-group data). Depending on the distribution, values are expressed as median and range (minimum–maximum) or as mean ± SD.

GraphPad Prism (version 8.0 Software; RRID: SCR_002798) or CSS Statistical software (StatSoft) were employed to perform statistical analysis.

Data availability

The data generated in this study are available within the article and its Supplementary Data files or from the corresponding author upon request.

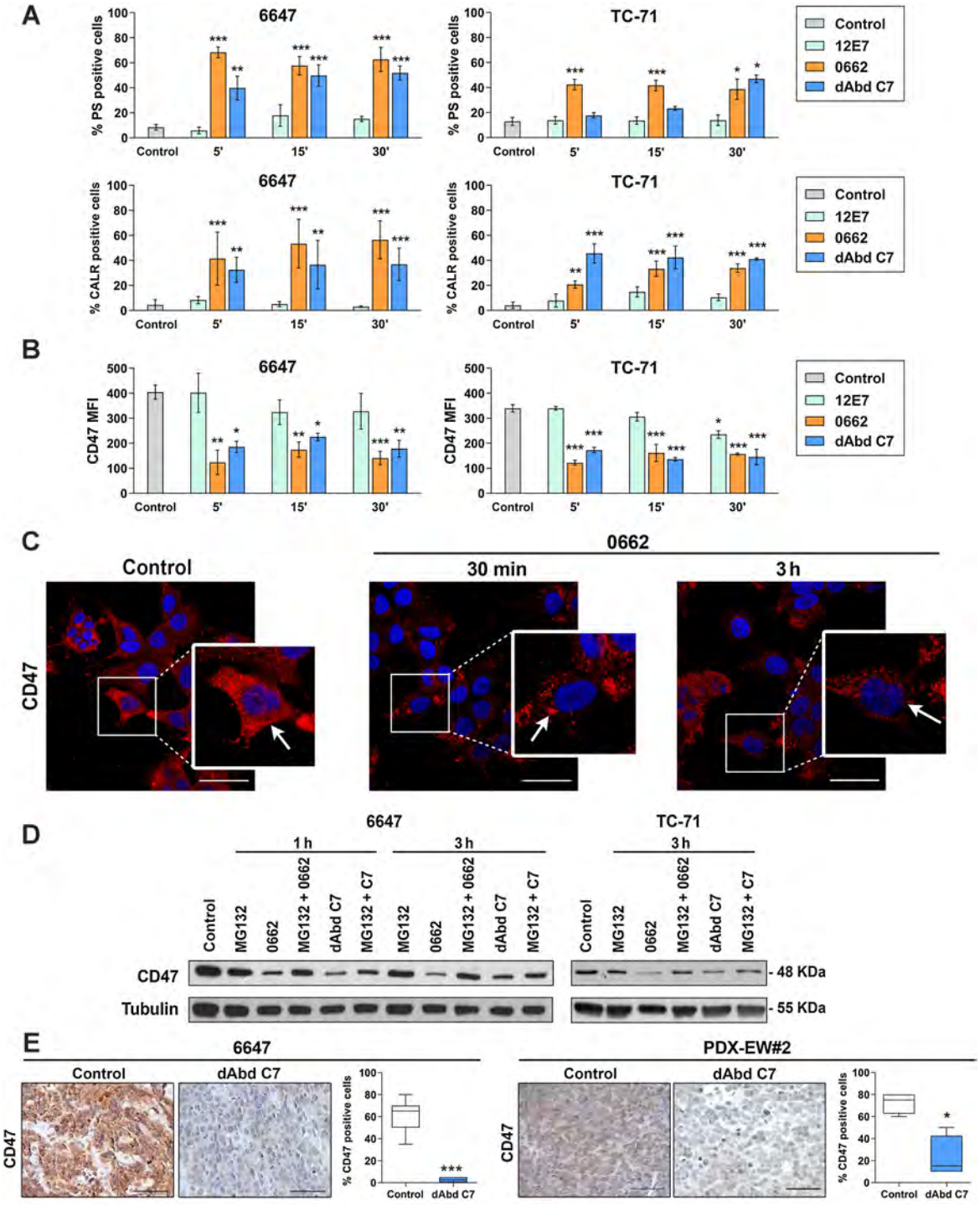

Figure 3.

Modulation of 'eat-me' and 'don't eat-me' molecules on EWS cell surface after CD99 engagement. **A,** Cytofluorimetric profile of PS and CALR expression in EWS cells treated with anti-CD99 antibodies (expressed as percentage of positive cells). **B,** MFI of CD47 expression in EWS cells treated with anti-CD99 antibodies. All cells are 100% positive to CD47 even after treatments. Bars indicated the mean ± SD of at least three independent experiments. One-way ANOVA: *, $P < 0.05$; **, $P < 0.01$; ***, $P < 0.001$. Gating strategy and representative profiles of each type of experiment (**A**–**B**), are reported in Supplementary Figs. S4 and S5. **C,** Confocal microscopy images of CD47 in TC-71 cells treated with 0662 mAb (10 μg/mL), indicating intracellular localization of CD47 (arrows). Enlarged views of the boxed regions are also displayed (scale bar, 50 μm, representative images of two independent experiments are shown). **D,** Western blot analysis of CD47 on total cell lysates from 6647 and TC-71 cells treated with anti-CD99 antibodies (0662 mAb; dAbd C7) in the presence or absence of the proteasome inhibitor MG132. Data are representative of at least three independent experiments. Beta-tubulin was included as loading control. **E,** Representative images of IHC staining of CD47 in 6647 (left) or PDX-EW#2 (right) xenografts after treatment with dAbd C7 (scale bar, 50 μm). Histograms represent the percentage of CD47 positive cells calculated after evaluation of at least ten fields. Data are presented as the median and range (minimum–maximum). Mann–Whitney U test: *, $P < 0.05$; ***, $P < 0.001$.

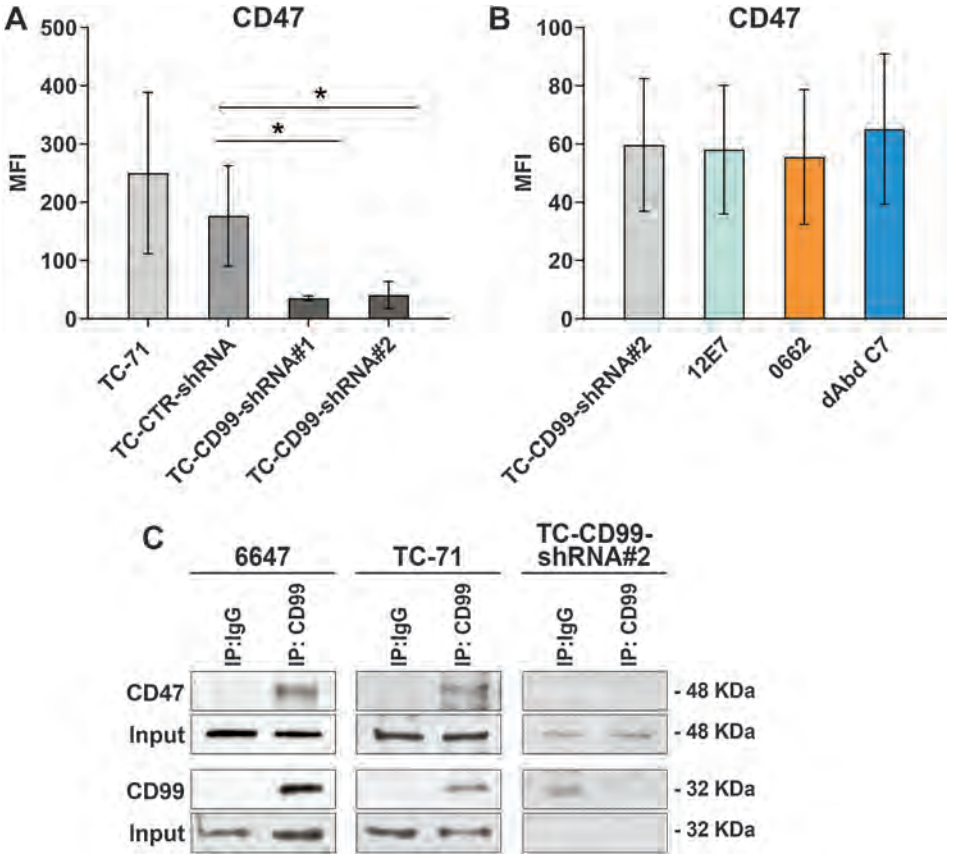

Figure 4.

The presence of CD99 on EWS cell surface influences CD47 status. **A,** Expression of CD47 in CD99-silenced cells. Bars indicate MFI. Mean ± SD of at least three independent experiments, Kruskal–Wallis test: *, $P < 0.05$. **B,** Cytofluorimetric profile of CD47 expression in TC-CD99-shRNA#2 EWS cells treated with anti-CD99 antibodies. Bars indicate the mean ± SD of at least three independent experiments. Gating strategy and representative profiles of each type of experiment (**A** and **B**), are reported in Supplementary Fig. S7. **C,** Immunoprecipitation of CD99 with CD47 in 6647, TC-71, and TC-CD99-shRNA#2 EWS cells. Blots are representative of at least three independent experiments.

Results

The human anti-CD99 dAbd C7 induces EWS cell death and recruitment of murine macrophages *in vivo*

For *in vivo* studies we used the human anti-CD99 dAbd C7, which is a diabody lacking an Fc that is capable of recognizing either human or mouse CD99 (ref. 6; Supplementary Fig. S1). In two *in vivo* experiments, one with the human patient-derived 6647 cell line (8) and the other with the PDX-EW#2 (11), mice were randomized to receive peritumoral human anti-CD99 dAbd C7, whereas control mice were not treated or received vehicle. In addition, in a third experiment, mice received the implant of PDX-EW#3 and were treated systemically by intraperitoneal injection of dAbd C7 (35). In all cases, after treatment with dAbd C7, a decrease in EWS tumor volume was observed (**Fig. 1A**; Supplementary Fig. S2A) and the mechanism responsible for this antitumor effect was studied (8, 11).

By histologic examination, slides of treated tumors (representative images from two mice/group) showed an increased number of cells with nuclear condensation of chromatin that is characteristic of programmed cell death (**Fig. 1B**; Supplementary Fig. S2B). In addition, we observed increased infiltration of murine F4/80^{+} macrophages inside the tumor (**Fig. 1C**; Supplementary Fig. S2C), indicating that triggering CD99 in EWS cells promoted macrophage recruitment, as expected when dying cells are visible by standard histologic techniques (41), and may activate the dynamic machinery of phagocytosis.

Ligation of CD99 on EWS cells induces their phagocytosis by macrophages

Human M0-like macrophages differentiated *ex vivo* from circulating monocytes (Supplementary Fig. S3) were used in a coculture model to investigate the elimination of EWS cells throughout the study, although some validations were also performed using M2-like polarized macrophages. Direct cocultures of M0-like macrophages with EWS cells treated with different anti-CD99 antibodies showed a significant increase in the phagocytic index compared with negative controls (**Fig. 2A** and **B**; Supplementary videos S1-S4). The phagocytic indices observed after exposure to the murine 0662 mAb or human dAbd C7 were significantly higher than that observed when tumor cells were exposed to the murine 12E7 mAb. Accordingly, the ligation of CD99 with the 0662 mAb or dAbd C7 in TC-71 cells significantly increased their elimination by macrophages (**Fig. 2C**); results showed that, when in cocultures, TC-71 cell survival reduced up to 30% to 50% after treatment with the 0662 mAb or dAbd C7 but cells maintained 80% to 90% of survival after exposure to the irrelevant, isotype control mAb MOPC-21 or to the anti-CD99 12E7 mAb. Thus, the removal of EWS cells by M0-like macrophages after ligation of CD99 seems to depend mainly on differences in the mechanisms of action of the Abs, rather than on Fc-dependent phagocytosis. This is in line with previous studies on CD99 (42, 43), a molecule that displays different epitopes recognized by different antibodies with distinct functions (1).

Triggering of CD99 by the 0662 mAb or by dAbd C7 has been demonstrated to lead to PS translocation from the cytoplasm to the exofacial layer of the plasma membrane within minutes after CD99 ligation, ultimately delivering caspase-independent cell death signaling (7–9). Exposed PS is a potent "eat me" signal, acting via direct interaction with PS receptors on phagocytes or indirectly through bridging molecules (44), and we confirmed PS exposure after treatment with 0662 mAb and dAbd C7, but not with 12E7 mAb (**Fig. 3A**; Supplementary Fig. S4 and Supplementary Fig. S5). In

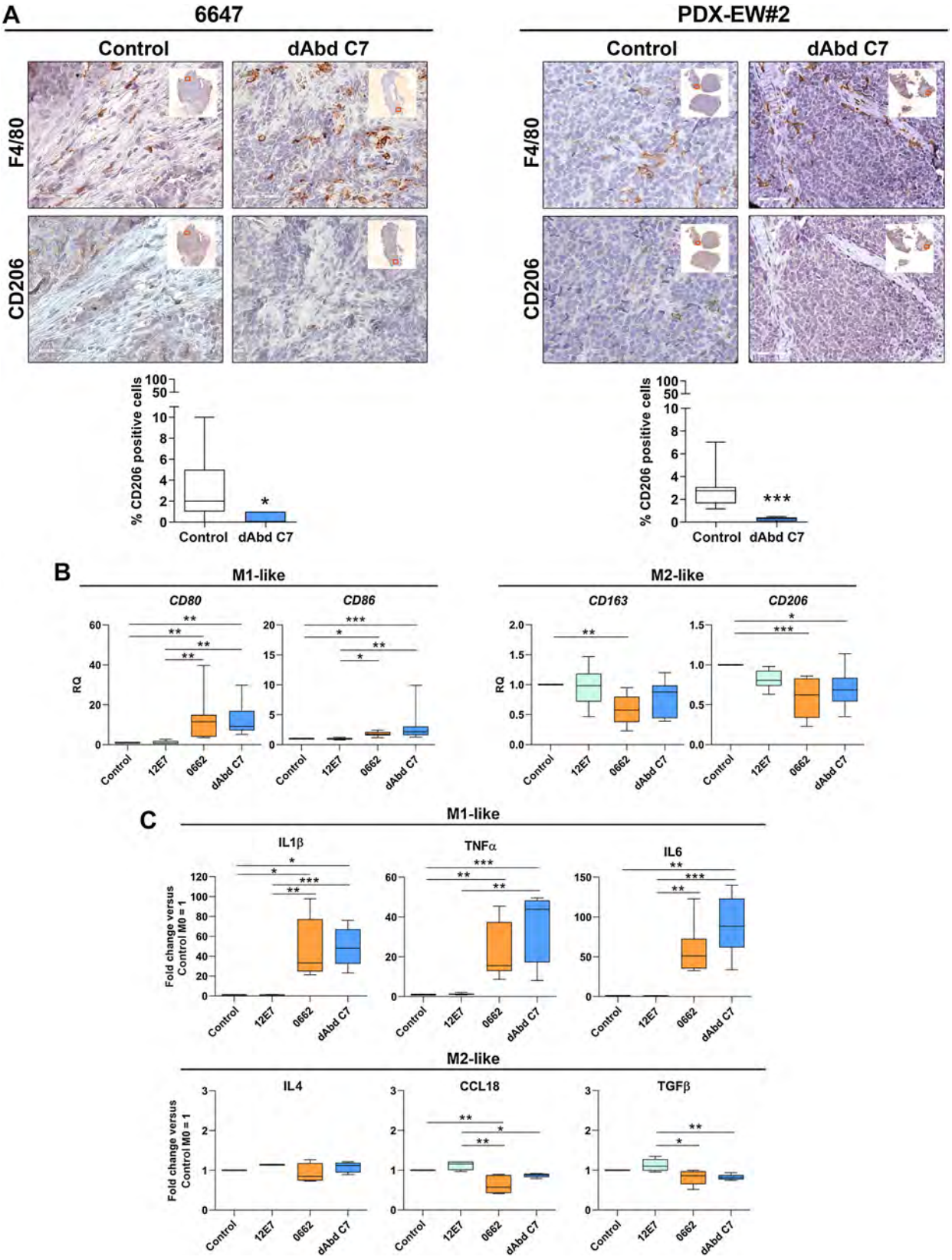
A
6647
PDX-EW#2
Control
dAbd C7
F4/80
CD206
% CD206 positive cells
B
M1-like
M2-like
CD80
CD86
CD163
CD206
RQ
Control
12E7
0662
dAbd C7
C
M1-like
IL1β
TNFα
IL6
Fold change versus Control M0 = 1
M2-like
IL4
CCL18
TGFβ

addition to PS, dying cells expose other "eat-me" signals on their surface, such as the endoplasmic reticulum chaperone calreticulin (CALR), which is normally confined to the cytosolic side of the cell membrane but may be expressed on the surface of dying cells under certain programmed cell death-inducing conditions, leading to cell phagocytosis (45). The induction of CALR exposure on the surface of EWS cells was observed when cells were exposed to 0662 mAb and human dAbd C7 but not 12E7 mAb (**Fig. 3A**; Supplementary Fig. S4 and Supplementary Fig. S5). The process was rapid, detectable as soon as 5 to 15 minutes after treatment, and was in parallel with PS exposure.

We next assessed whether anti-CD99 induced alterations in the expression of 'don't eat me' signals, such as CD47, which is believed to act as an anti-phagocytic marker (46). CD47 is highly expressed in multiple types of human cancer cells, allowing them to escape phagocytosis by macrophages (47). Here, we confirmed that EWS cells generally express high levels of CD47 (a panel of nine human patient-derived cell lines was tested: Supplementary Fig. S6). Overall, the average expression of CD47 on the EWS cells was significantly higher than it was on hBM-MSCs, which are thought to be the putative cell of origin of EWS cells (48). After CD99 engagement with 0662 mAb and dAbd C7, but not with 12E7 mAb, CD47 expression was significantly and quickly reduced on the surface of EWS cells (**Fig. 3B**; Supplementary Fig. S4 and Supplementary Fig. S5). Confocal microscopy of CD47 on adherent cells after CD99 ligation showed progressive disappearance of CD47 from the cell surface and cytoplasm (**Fig. 3C**), suggesting that CD47 was internalized and then degraded inside EWS cells. Indeed, Western blotting of cells exposed to 0662 mAb or dAbd C7 for 1 to 3 hours confirmed CD47 downregulation (**Fig. 3D**). This decreased expression was partly due to proteasome-dependent degradation, as demonstrated by its rescue using the proteasome inhibitor MG132 *in vitro* (**Fig. 3D**). The reduction of CD47 expression was also confirmed *in vivo* in xenografts treated with the dAbd C7 (**Fig. 3E**).

The functional relationship between CD99 and CD47 was further demonstrated in EWS cells in which CD99 was silenced (3). In these cells, expression of CD47 was significantly lower than that in the parental cells (**Fig. 4A**; Supplementary Fig. S7). In addition, treatment of these cells with anti-CD99 did not induce CD47 depletion from the cell surface (**Fig. 4B**; Supplementary Fig. S7) or exposure of PS and CALR (Supplementary Fig. S8). Immunoprecipitation of CD99 with CD47 was demonstrated in parental 6647 and TC-71 cells but not in CD99-silenced TC-CD99-shRNA#2 EWS cells (**Fig. 4C**). Thus, our data support the hypothesis that CD99 interacts with CD47 after ligation, causing its internalization and favoring phagocytosis by macrophages.

A decrease of approximately one third in surface CD47 was previously reported to be effective in promoting tumor-cell phagocytosis by macrophages, regardless of the macrophage subtype (49). Consistent with this, we observed that when M0-like macrophages (**Fig. 2**) or M2-like macrophages (Supplementary Fig. S9) were used in coculture with EWS cells, only if the cells were pretreated with 0662 mAb or dAbd C7, reducing CD47 levels, was the phagocytic index enhanced and EWS cells eliminated.

Ligation of CD99 on macrophages induces their polarization toward a M1-like phenotype

Enlarged images of treated xenografts (**Fig. 1C**) showed EWS cell phagocytosis by macrophages. Therefore, we decided to analyze in more detail the infiltration of tumor-associated macrophages and the association between dying cells and the phagocytes. We found that the anti-CD99 dAbd C7 can recognize murine CD99 on macrophages by using a cell population derived from peritoneal lavage of NSG mice double stained for F4/80 (expressed in monocytes and macrophages) and CD99 to verify that both markers are expressed on the plasma membrane of these cells (Supplementary Fig. S1B). In untreated xenograft tumors, some of the few infiltrating F4/80$^+$ macrophages also expressed CD206, a major marker for anti-inflammatory M2-like macrophages (50) (**Fig. 5A**). In contrast, infiltrating macrophages of tumors treated with dAbd C7 lacked the CD206 marker (**Fig. 5A**).

Ex vivo qPCR analysis confirmed that coculturing of anti-CD99–treated EWS cells with M0-like macrophages caused the upregulation of genes that are usually associated with a pro-inflammatory M1-phenotype, such as those encoding *CD80, CD86, IL1β, IL6*, and *TNFα* (**Fig. 5B** and **C**; Supplementary Table S2), and the downregulation of genes associated with an M2-phenotype, such as those encoding *CD163* and *CD206* (**Fig. 5B**; Supplementary Table S2), together with increased expression and release of IL1β, IL6, and TNFα (M1-like cytokines) and a decrease in release of CCL18 and TGFβ (M2-like cytokines; **Fig. 5B**; Supplementary Table S2). Similar data were also obtained when *ex vivo* M2-like macrophages were used (Supplementary Fig. S10; Supplementary Table S2).

Because CD99 is expressed in several immune cells, including macrophages (31), it is possible that the anti-CD99 present on EWS-pretreated cells can also deliver signals to macrophages in direct cell cocultures. Therefore, we first confirmed that CD99 is expressed on human macrophages—M0, M1, and M2-like macrophages—at relevant levels (Supplementary Fig. S11) and then evaluated the effects of CD99 engagement on these immune cells. Anti-CD99 did not deliver a cell death message in macrophages, which is consistent with our previous evidence in normal stem cells (8, 51), but rather they increased the phagocytic capacity of these scavenger cells (**Fig. 6A**), which led to significant reduction in EWS cell survival in coculture experiments (**Fig. 6B**).

In addition, M0-like cells exposed to the anti-CD99 0662 mAb or dAbd C7 showed increased expression of the M1-like markers *CD80, CD86, IL1β, IL6*, and *TNFα* but decreased expression of the M2-like marker *CD206* and *IL4* (**Fig. 6C** and **D**). Consistent with this, both 0662 mAb and dAbd C7 triggered activation of the phospho-signal transducers and activators of transcription (STAT)-1, and enhanced levels of Fos and Jun, which are components of the AP-1 complex (**Fig. 6E**), further supporting the hypothesis that these CD99 antibodies promote macrophage polarization toward the M1-like phenotype.

Figure 5.

Ex vivo undifferentiated M0-like macrophages switch to M1-like phenotype when cocultured with EWS cells treated with agonistic anti-CD99 antibodies. **A,** Representative IHC images of murine F4/80$^+$ and CD206$^+$ macrophages in 6647 (left) and PDX-EW#2 (right) xenografts after treatment with dAbd C7 (scale bar, 50 μm). Low magnifications are inserted to show tumor morphology, and the box represents the field of view of the 40× images displayed for each antigen. Quantification of IHC staining of tumor tissue samples in each group were quantified by ImageJ software. Data are expressed as median and range (minimum–maximum). Mann–Whitney U test: *, $P < 0.05$; ***, $P < 0.001$. **B,** The relative expression of *CD80, CD86, CD163, CD206* was analyzed by qPCR in M0-like macrophages cocultured with TC-EGFP cells treated with 0662 mAb or dAbd C7 as indicated in material and methods. Data are expressed as the median and range (minimum–maximum). Kruskal–Wallis test: *, $P < 0.05$; **, $P < 0.01$; ***, $P < 0.001$. **C,** Multiplex cytokine assay analysis of IL1β, IL6, TNFα, CCL18, TGFβ1, and IL4 release in M0-like macrophages cocultured with TC-71 EGFP cells treated with 0662 mAb or dAbd C7 as indicated in material and methods. Data are expressed as the median and range (minimum–maximum) of the fold increase versus control = 1. Kruskal–Wallis test: *, $P < 0.05$; **, $P < 0.01$; ***, $P < 0.001$.

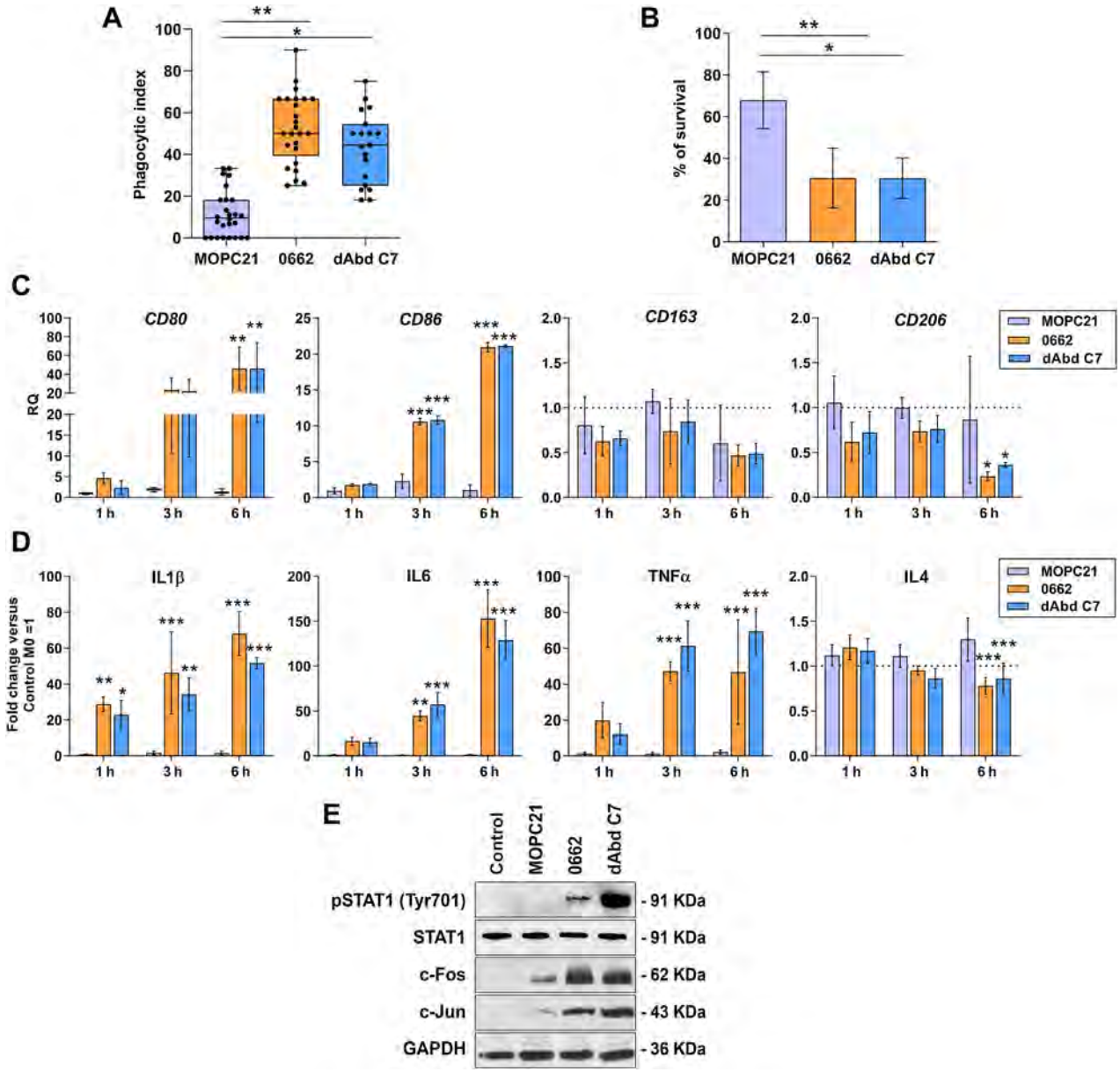

Figure 6.

Engagement of CD99 on *ex vivo* undifferentiated M0-like macrophages induces M1-like polarization and increases their phagocytosis capabilities against EWS cells. **A,** Phagocytic index of M0-like macrophages exposed to anti-CD99 antibodies (0662 mAb; dAbd C7) or to irrelevant MOPC21 antibody (used as isotype control) for 3 hours and then cocultured with TC-EGFP cells for an additional 3 hours as indicated in the Materials and Methods. The phagocytic index indicates the number of EWS cells phagocytosed per 100 macrophages. Dots represent single fields, and data are expressed as the median and range (minimum–maximum) of at least three independent experiments. Kruskal–Wallis test: *, $P < 0.05$; **, $P < 0.01$. **B,** TC-EGFP cell survival in the presence of M0-like macrophages exposed to anti-CD99 antibodies. Trypan blue vital cell count was used. Data are expressed as percentages compared with untreated EWS cells. Bars indicate mean ± SD from at least three independent experiments. Kruskal–Wallis test: *, $P < 0.05$; **, $P < 0.01$. **C,** Relative expression of *CD80, CD86, CD163*, and *CD206* was analyzed by qPCR in M0-like macrophages treated with anti-CD99 0662 mAb or dAbd C7 for 1 to 6 hours. Data are expressed as the mean ± SD. Two-way ANOVA test: *, $P < 0.05$; **, $P < 0.01$; ***, $P < 0.001$. **D,** Multiplex cytokine assay analysis of IL1β, IL6, TNFα, and IL4 release in M0-like macrophages treated with anti-CD99 0662 mAb or dAbd C7 as indicated in the Materials and Methods. Data are expressed as mean ± SD of the fold increase versus control M0-like = 1. Two-way ANOVA test: *, $P < 0.05$; **, $P < 0.01$; ***, $P < 0.001$. **E,** Western blot analysis of intracellular signaling molecules in M0-like macrophages treated as indicated. GAPDH was used as the loading control. Representative blots from three independent experiments are shown.

Discussion

Immune checkpoint inhibitors have radically changed treatment for many types of cancer, but their clinical application has been limited by a low response rate, especially in tumors that are characterized by scarce infiltration of functional cytotoxic T lymphocytes into the tumor bed and an uninflamed phenotype (52). EWS is a nonimmunogenic tumor with a low mutational burden (53) and it has an

immunosuppressive TME with few, if any, functional T cells (54), mature dendritic cells (DC), and pro-inflammatory M1 macrophages (27); rather, it features substantial myeloid-cell infiltration (55), including immature (M0-like) and immunosuppressive (M2-like) macrophages (27, 29). The abundance of M0/M2-like macrophages has been reported to be relevant to the progression of EWS (30, 56). Fujiwara and colleagues found that macrophages in the TME were able to induce angiogenesis and osteoclast activation to promote EWS progression (30). More recently, EWS cells were found to inhibit the differentiation of DCs by secreting exosomes, resulting in the formation of an immunosuppressive TME, and weakened adaptive immunity (57). Reshaping the TME through the modulation of macrophage functions appears to be an interesting perspective in EWS.

In our study, we offer a strategy to reeducate M0/M2-like macrophages and modify the TME to combat cancer. We demonstrate that triggering CD99, a cell-surface molecule highly expressed in EWS cells, but also present on macrophages, induced phagocytosis by macrophages to exert antitumor effects; and polarization of M0/M2-like macrophages toward the M1 phenotype. Macrophage-mediated phagocytosis contributes to the efficacy of mAb therapies because macrophages express all classes of Fcγ receptors, thus having the potential to destroy tumors via antibody-dependent phagocytosis (50). However, when EWS cells were treated with the agonistic anti-CD99 0662 mAb or the human dAbd C7, we observed a significant increase in tumor-cell phagocytosis by macrophages compared with Fc-dependent phagocytosis alone, most likely influenced by the redistribution of PS and CALR, two 'eat-me' signals, and by the decrease in the expression of CD47, a 'do-not-eat-me' signal, on EWS cell membranes minutes after CD99 ligation. Thus, in the treated cells, 'eat-me' signals prevailed, driving EWS cell engulfment and phagocytosis by macrophages.

Targeting CD47 to enhance macrophage phagocytosis has emerged as a promising strategy for tumor immunotherapy (58); however, its efficacy in solid tumors is still limited. Here, we indicate another mechanism to block CD47 inhibitory functions: when engaged, CD99 interacts with CD47 and induces its internalization and ubiquitination, thus inhibiting its expression in tumor cells. Because the expression of CD99 at high levels is confined to a few cell types (1), this approach may selectively direct CD47 blockade to cancer target cells, thereby improving the safety of CD47 blocking therapy.

A decrease in CD47 expression was observed *in vivo* when EWS xenografts were treated with human anti-CD99 dAbd C7. The absence of murine immunocompetent models for EWS limited our understanding of the crosstalk between tumor cells and different immune cell populations. However, because EWS xenografts in NSG mice lack T and NK cells but retain myeloid cells, our data further support the importance of macrophages in the therapeutic control of EWS tumor growth. We acknowledge that a limitation of this study is the reliance on subcutaneous EWS tumors, which lack elements of the bone microenvironment and may be less informative than orthotopic models. The influence of the implantation site on the composition of the tumor immune infiltrate in preclinical models is poorly understood, and this aspect should be considered when conducting preclinical studies with immunotherapeutic agents. However, when *Goldstein SD* and collaborators (59) compared macrophage infiltration in three subcutaneous EWSs and three orthotopic EWSs, they found that subcutaneous tumors were more actively infiltrated by macrophages with modest M2 polarization than orthotopic tumors, allowing these cells to be evaluated in the context of the TME. In a variety of tumors, *Denis M* and collaborators have recently shown that although there are several differences between subcutaneous and orthotopic models at baseline, immunotherapy can induce a homogeneous immune infiltrate regardless of the site of implantation, suggesting that the post-therapeutic infiltrate is determined by the effect of therapy on immune cell recruitment or activation rather than the composition of the preexisting immune infiltrate (60). In addition to inducing methuosis, a nonapoptotic form of cell death due to excessive intracellular accumulation of vacuoles (7), our data indicate that targeting CD99 results in increased numbers of macrophages, enhanced phagocytosis, and inhibition of tumor growth. Furthermore, anti-CD99 can reprogram *ex vivo* undifferentiated M0-like macrophages or M2-polarized macrophages toward an M1-like phenotype. As the most abundant immune cells in the TME of EWS, this finding is of paramount importance because M1-like and M2-like macrophages represent the two extremes of a continuum in a universe of activation states. Classically activated M1-like macrophages produce many pro-inflammatory and effector molecules and exert antitumor cytolytic activity, whereas alternatively activated M2-like macrophages are anti-inflammatory and promote wound healing, angiogenesis, and tissue remodeling, ultimately favoring tumor invasion and progression (61). Triggering of CD99 in macrophages induces secretion of the chemokines IL1β, IL6, and TNFα and expression of the markers CD80 and CD86, all of which are markers of the M1-like phenotype.

Taken together, our data indicate that CD99 can be a dual-use modulator against EWS cells, inducing tumor cell death and rapid clearance of dying cells by phagocytosis. On the other hand, it reeducates macrophages, promoting their pro-inflammatory functions and enhancing their antitumor response. The result is tumor growth inhibition, supporting the idea that targeting CD99 can be considered a macrophage-targeted therapy.

Authors' Disclosures

M.C. Manara reports grants from Italian Association for Cancer Research (AIRC) during the conduct of the study, grants from ERANET TRANSCAN-2_TORPEDO, and nonfinancial support and other support from Diatheva Srl outside the submitted work. C. Manferdini reports grants from AIRC during the conduct of the study. C. Cristalli reports grants from AIRC during the conduct of the study, grants from ERANET TRANSCAN-2_TORPEDO, and nonfinancial support and other support from Diatheva Srl outside the submitted work. M. Carrabotta reports grants from AIRC during the conduct of the study, grants from ERANET TRANSCAN-2_TORPEDO, Italian Ministry of Health; and nonfinancial support and other support from Diatheva Srl outside the submitted work. A. De Feo reports grants from AIRC during the conduct of the study, grants from ERANET TRANSCAN-2_TORPEDO and the Italian Ministry of Health, and nonfinancial support and other support from Diatheva Srl outside the submitted work. G. Caldoni reports grants from AIRC during the conduct of the study, grants from ERANET TRANSCAN-2_TORPEDO, other support from Onlus il Pensatore: Matteo Amitrano; Aurora Tomaselli, ricerca e prevenzione; Liberi di vivere, Luca Righi; Chiara Paradiso-la forza dell'amore onlus; Associazione Mario Campanacci; and Associazione "Un sorriso con Luca"; and nonfinancial support and other support from Diatheva Srl outside the submitted work. M. Pasello reports grants from AIRC during the conduct of the study, grants from ERANET TRANSCAN-2_TORPEDO, and nonfinancial support from Diatheva Srl outside the submitted work. L. Landuzzi reports grants from AIRC during the conduct of the study, grants from ERANET TRANSCAN-2_TORPEDO, and nonfinancial support and other support from Diatheva Srl outside the submitted work. M. Magnani reports other support from Diatheva Srl during the conduct of the study and other support from Diatheva Srl outside the submitted work. G. Lisignoli reports grants from AIRC during the conduct of the study. K. Scotlandi reports grants from AIRC during the conduct of the study, grants from ERANET TRANSCAN-2_TORPEDO, and nonfinancial support and other support from Diatheva Srl outside the submitted work; in addition, K. Scotlandi has a patent 0001397621 licensed to Diatheva Srl. No disclosures were reported by the other authors.

Authors' Contributions

M.C. Manara: Conceptualization, data curation, writing–original draft, writing–review and editing, analysis and interpretation of data, graphed the data.

C. Manferdini: Conceptualization, data curation, writing–review and editing, data acquisition, analysis and interpretation of data, graphed the data. **C. Cristalli:** Data curation, writing–review and editing, data acquisition, analysis and interpretation of data, graphed the data. **M. Carrabotta:** Data curation, writing–review and editing, data acquisition, analysis and interpretation of data. **S. Santi:** Data curation, writing–review and editing, data acquisition, analysis and interpretation of data. **A. De Feo:** Data curation, writing–review and editing, data acquisition, analysis and interpretation of data. **G. Caldoni:** Data curation, writing–review and editing, data acquisition, analysis and interpretation of data. **M. Pasello:** Data curation, writing–review and editing, data acquisition. **L. Landuzzi:** Data curation, writing–review and editing, data acquisition, analysis and interpretation of data. **P.-L. Lollini:** Resources, writing–review and editing. **F. Salamanna:** Data curation, writing–review and editing, data acquisition. **S. Dominici:** Data curation, writing–review and editing, data acquisition. **V. Fiori:** Resources, writing–review and editing. **M. Magnani:** Resources, writing–review and editing. **G. Lisignoli:** Conceptualization, resources, data curation, supervision, writing–original draft, writing–review and editing, analysis and interpretation of data, graphed the data. **K. Scotlandi:** Conceptualization, resources, data curation, supervision, writing–original draft, writing–review and editing.

Acknowledgments

The authors thank Cristina Ghinelli for editing the figures and Luca Cattini for Flow Cytometry support. The authors are grateful to the following associations for funding the scholarship of G. Caldoni for the PhD in Oncology, Hematology and Pathology at the University of Bologna: Onlus il Pensatore 'Matteo Amitrano,' Aurora Tomaselli, ricerca e prevenzione, Liberi di vivere, 'Luca Righi,' 'Chiara Paradiso' – la forza dell'amore onlus, Associazione Mario Campanacci, and Associazione 'Un sorriso con Luca'.

The research leading to these results received funding from Fondazione AIRC per la ricerca sul cancro ETS under IG2016–18451 and IG2019–22805 (K. Scotlandi). The research also received support for the establishment of PDX modeling by funds from the European Union (ERANET TRANSCAN-2_TORPEDO ER-2015–2360405 to K. Scotlandi).

The publication costs of this article were defrayed in part by the payment of publication fees. Therefore, and solely to indicate this fact, this article is hereby marked "advertisement" in accordance with 18 USC section 1734.

Note

Supplementary data for this article are available at Cancer Immunology Research Online (http://cancerimmunolres.aacrjournals.org/).

Received May 26, 2023; revised September 30, 2023; accepted December 1, 2023; published first December 4, 2023.

References

1. Pasello M, Manara MC, Scotlandi K. CD99 at the crossroads of physiology and pathology. J Cell Commun Signal 2018;12:55–68.
2. Grunewald TGP, Cidre-Aranaz F, Surdez D, Tomazou EM, de Alava E, Kovar H, et al. Ewing sarcoma. Nat Rev Dis Primers 2018;4:5.
3. Rocchi A, Manara MC, Sciandra M, Zambelli D, Nardi F, Nicoletti G, et al. CD99 inhibits neural differentiation of human Ewing sarcoma cells and thereby contributes to oncogenesis. J Clin Invest 2010;120:668–80.
4. Balestra T, Manara MC, Laginestra MA, Pasello M, De Feo A, Bassi C, et al. Targeting CD99 compromises the oncogenic effects of the chimera EWS-FLI1 by inducing reexpression of zyxin and inhibition of GLI1 activity. Mol Cancer Ther 2022;21:58–69.
5. Manara MC, Pasello M, Scotlandi K. CD99: a cell surface protein with an oncojanus role in tumors. Genes 2018;9:159.
6. Moricoli D, Carbonella DC, Dominici S, Fiori V, Balducci MC, Guerzoni C, et al. Process development of a human recombinant diabody expressed in *E. coli*: engagement of CD99-induced apoptosis for target therapy in Ewing's sarcoma. Appl Microbiol Biotechnol 2016;100:3949–63.
7. Manara MC, Terracciano M, Mancarella C, Sciandra M, Guerzoni C, Pasello M, et al. CD99 triggering induces methuosis of Ewing sarcoma cells through IGF-1R/RAS/Rac1 signaling. Oncotarget 2016;7:79925–42.
8. Guerzoni C, Fiori V, Terracciano M, Manara MC, Moricoli D, Pasello M, et al. CD99 triggering in Ewing sarcoma delivers a lethal signal through p53 pathway reactivation and cooperates with doxorubicin. Clin Cancer Res 2015;21:146–56.
9. Cerisano V, Aalto Y, Perdichizzi S, Bernard G, Manara MC, Benini S, et al. Molecular mechanisms of CD99-induced caspase-independent cell death and cell–cell adhesion in Ewing's sarcoma cells: actin and zyxin as key intracellular mediators. Oncogene 2004;23:5664–74.
10. Scotlandi K, Perdichizzi S, Bernard G, Nicoletti G, Nanni P, Lollini PL, et al. Targeting CD99 in association with doxorubicin: an effective combined treatment for Ewing's sarcoma. Eur J Cancer 2006;42:91–6.
11. Nanni P, Landuzzi L, Manara MC, Righi A, Nicoletti G, Cristalli C, et al. Bone sarcoma patient-derived xenografts are faithful and stable preclinical models for molecular and therapeutic investigations. Sci Rep 2019;9:12174.
12. Shin YK, Lee GK, Kook MC, Jung KC, Kim JR, Song HG, et al. Reduced expression of CD99 and functional disturbance in anencephalic cortical thymocytes. Virchows Arch 1999;434:443–9.
13. Bernard G, Breittmayer JP, de Matteis M, Trampont P, Hofman P, Senik A, et al. Apoptosis of immature thymocytes mediated by E2/CD99. J Immunol 1997;158:2543–50.
14. Bernard G, Zoccola D, Deckert M, Breittmayer JP, Aussel C, Bernard A. The E2 molecule (CD99) specifically triggers homotypic aggregation of $CD4^+$ $CD8^+$ thymocytes. J Immunol 1995;154:26–32.
15. Pettersen RD, Bernard G, Olafsen MK, Pourtein M, Lie SO. CD99 signals caspase-independent T cell death. J Immunol 2001;166:4931–42.
16. Szondy Z, Garabuczi E, Toth K, Kiss B, Koroskenyi K. Thymocyte death by neglect: contribution of engulfing macrophages. Eur J Immunol 2012;42:1662–7.
17. Aussel C, Bernard G, Breittmayer JP, Pelassy C, Zoccola D, Bernard A. Monoclonal antibodies directed against the E2 protein (MIC2 gene product) induce exposure of phosphatidylserine at the thymocyte cell surface. Biochemistry 1993;32:10096–101.
18. Kim SH, Choi EY, Shin YK, Kim TJ, Chung DH, Chang SI, et al. Generation of cells with Hodgkin's and Reed–Sternberg phenotype through downregulation of CD99 (Mic2). Blood 1998;92:4287–95.
19. Scotlandi K, Baldini N, Cerisano V, Manara MC, Benini S, Serra M, et al. CD99 engagement: an effective therapeutic strategy for Ewing tumors. Cancer Res 2000;60:5134–42.
20. Locati M, Curtale G, Mantovani A. Diversity, mechanisms, and significance of macrophage plasticity. Annu Rev Pathol 2020;15:123–47.
21. Surh CD, Sprent J. T-cell apoptosis detected in situ during positive and negative selection in the thymus. Nature 1994;372:100–3.
22. Garabuczi E, Kiss B, Felszeghy S, Tsay GJ, Fesus L, Szondy Z. Retinoids produced by macrophages engulfing apoptotic cells contribute to the appearance of transglutaminase 2 in apoptotic thymocytes. Amino Acids 2013;44:235–44.
23. Koroskenyi K, Duro E, Pallai A, Sarang Z, Kloor D, Ucker DS, et al. Involvement of adenosine A2A receptors in engulfment-dependent apoptotic cell suppression of inflammation. J Immunol 2011;186:7144–55.
24. Szondy Z, Sarang Z, Molnar P, Nemeth T, Piacentini M, Mastroberardino PG, et al. Transglutaminase 2-/- mice reveal a phagocytosis-associated crosstalk between macrophages and apoptotic cells. Proc Natl Acad Sci USA 2003;100:7812–7.
25. Altvater B, Kailayangiri S, Perez Lanuza LF, Urban K, Greune L, Flugge M, et al. HLA-G and HLA-E immune checkpoints are widely expressed in Ewing sarcoma but have limited functional impact on the effector functions of antigen-specific CAR T cells. Cancers 2021;13:2857.
26. Morales E, Olson M, Iglesias F, Dahiya S, Luetkens T, Atanackovic D. Role of immunotherapy in Ewing sarcoma. J Immunother Cancer 2020;8:e000653.
27. Stahl D, Gentles AJ, Thiele R, Gutgemann I. Prognostic profiling of the immune cell microenvironment in Ewing s sarcoma family of tumors. Oncoimmunology 2019;8:e1674113.
28. Thakur MD, Franz CJ, Brennan L, Brouwer-Visser J, Tam R, Korski K, et al. Immune contexture of pediatric cancers. Eur J Cancer 2022;170:179–93.
29. Vakkila J, Jaffe R, Michelow M, Lotze MT. Pediatric cancers are infiltrated predominantly by macrophages and contain a paucity of dendritic cells: a major nosologic difference with adult tumors. Clin Cancer Res 2006;12:2049–54.

30. Fujiwara T, Fukushi J, Yamamoto S, Matsumoto Y, Setsu N, Oda Y, et al. Macrophage infiltration predicts a poor prognosis for human Ewing sarcoma. Am J Pathol 2011;179:1157–70.
31. Schenkel AR, Mamdouh Z, Chen X, Liebman RM, Muller WA. CD99 plays a major role in the migration of monocytes through endothelial junctions. Nat Immunol 2002;3:143–50.
32. Nanni P, Nicoletti G, Landuzzi L, Croci S, Murgo A, Palladini A, et al. High metastatic efficiency of human sarcoma cells in Rag2/gammac double knockout mice provides a powerful test system for antimetastatic targeted therapy. Eur J Cancer 2010;46:659–68.
33. Percie du Sert N, Ahluwalia A, Alam S, Avey MT, Baker M, Browne WJ, et al. Reporting animal research: explanation and elaboration for the ARRIVE guidelines 2.0. PLoS Biol 2020;18:e3000411.
34. Nomura T, Tamaoki N, Takakura A, Suemizu H. Basic concept of development and practical application of animal models for human diseases. Curr Top Microbiol Immunol 2008;324:1–24.
35. Al Shoyaib A, Archie SR, Karamyan VT. Intraperitoneal route of drug administration: should it be used in experimental animal studies? Pharm Res 2019; 37:12.
36. Murray PJ, Allen JE, Biswas SK, Fisher EA, Gilroy DW, Goerdt S, et al. Macrophage activation and polarization: nomenclature and experimental guidelines. Immunity 2014;41:14–20.
37. Ghosn EE, Cassado AA, Govoni GR, Fukuhara T, Yang Y, Monack DM, et al. Two physically, functionally, and developmentally distinct peritoneal macrophage subsets. Proc Natl Acad Sci USA 2010;107:2568–73.
38. Gellini M, Ascione A, Flego M, Mallano A, Dupuis ML, Zamboni S, et al. Generation of human single-chain antibody to the CD99 cell surface determinant specifically recognizing Ewing's sarcoma tumor cells. Curr Pharm Biotechnol 2013;14:449–63.
39. Moricoli D, Laguardia ME, Carbonella DC, Balducci MC, Dominici S, Fiori V, et al. Isolation of a new human scFv antibody recognizing a cell surface binding site to CEACAM1. Large yield production, purification, and characterization in *E. coli* expression system. Protein Expr Purif 2014;93:38–45.
40. Manferdini C, Paolella F, Gabusi E, Gambari L, Piacentini A, Filardo G, et al. Adipose stromal cells mediated switching of the pro-inflammatory profile of M1-like macrophages is facilitated by PGE2: *in vitro* evaluation. Osteoarthritis Cartilage 2017;25:1161–71.
41. Leers MP, Bjorklund V, Bjorklund B, Jornvall H, Nap M. An immunohistochemical study of the clearance of apoptotic cellular fragments. Cell Mol Life Sci 2002;59:1358–65.
42. Gil MC, Lee MH, Seo JI, Choi YL, Kim MK, Jung KC, et al. Characterization and epitope mapping of two monoclonal antibodies against human CD99. Exp Mol Med 2002;34:411–8.
43. Jung KC, Kim NH, Park WS, Park SH, Bae Y. The CD99 signal enhances Fas-mediated apoptosis in the human leukemic cell line, Jurkat. FEBS Lett 2003;554: 478–84.
44. Lemke G. How macrophages deal with death. Nat Rev Immunol 2019;19:539–49.
45. Obeid M, Tesniere A, Ghiringhelli F, Fimia GM, Apetoh L, Perfettini JL, et al. Calreticulin exposure dictates the immunogenicity of cancer cell death. Nat Med 2007;13:54–61.
46. Huang J, Liu F, Li C, Liang X, Li C, Liu Y, et al. Role of CD47 in tumor immunity: a potential target for combination therapy. Sci Rep 2022;12:9803.
47. Jia X, Yan B, Tian X, Liu Q, Jin J, Shi J, et al. CD47/SIRPalpha pathway mediates cancer immune escape and immunotherapy. Int J Biol Sci 2021;17:3281–7.
48. Tirode F, Laud-Duval K, Prieur A, Delorme B, Charbord P, Delattre O. Mesenchymal stem cell features of Ewing tumors. Cancer Cell 2007;11:421–9.
49. Chao MP, Jaiswal S, Weissman-Tsukamoto R, Alizadeh AA, Gentles AJ, Volkmer J, et al. Calreticulin is the dominant pro-phagocytic signal on multiple human cancers and is counterbalanced by CD47. Sci Transl Med 2010;2:63ra94.
50. Mantovani A, Allavena P, Marchesi F, Garlanda C. Macrophages as tools and targets in cancer therapy. Nat Rev Drug Discov 2022;21:799–820.
51. Amaral AT, Manara MC, Berghuis D, Ordonez JL, Biscuola M, Lopez-Garcia MA, et al. Characterization of human mesenchymal stem cells from Ewing sarcoma patients. Pathogenetic implications. PLoS One 2014;9:e85814.
52. Zhang J, Huang D, Saw PE, Song E. Turning cold tumors hot: from molecular mechanisms to clinical applications. Trends Immunol 2022;43:523–45.
53. Grobner SN, Worst BC, Weischenfeldt J, Buchhalter I, Kleinheinz K, Rudneva VA, et al. The landscape of genomic alterations across childhood cancers. Nature 2018;555:321–7.
54. Machado I, Lopez-Guerrero JA, Scotlandi K, Picci P, Llombart-Bosch A. Immunohistochemical analysis and prognostic significance of PD-L1, PD-1, and $CD8^+$ tumor-infiltrating lymphocytes in Ewing's sarcoma family of tumors (ESFT). Virchows Arch 2018;472:815–24.
55. Zhang Z, Shi Y, Zhu Z, Fu J, Liu D, Liu X, et al. Characterization of myeloid signature genes for predicting prognosis and immune landscape in Ewing sarcoma. Cancer Sci 2023;114:1240–55.
56. Rossig C. Cellular immunotherapy strategies for Ewing sarcoma. Immunotherapy 2014;6:611–21.
57. Gassmann H, Schneider K, Evdokimova V, Ruzanov P, Schober SJ, Xue B, et al. Ewing sarcoma-derived extracellular vesicles impair dendritic cell maturation and function. Cells 2021;10:2081.
58. Takimoto CH, Chao MP, Gibbs C, McCamish MA, Liu J, Chen JY, et al. The macrophage 'DO not eat me' signal, CD47, is a clinically validated cancer immunotherapy target. Ann Oncol 2019;30:486–9.
59. Goldstein SD, Hayashi M, Albert CM, Jackson KW, Loeb DM. An orthotopic xenograft model with survival hindlimb amputation allows investigation of the effect of tumor microenvironment on sarcoma metastasis. Clin Exp Metastasis 2015;32:703–15.
60. Denis M, Mathe D, Micoud M, Choffour PA, Grasselly C, Matera EL, et al. Impact of mouse model tumor implantation site on acquired resistance to anti–PD-1 immune checkpoint therapy. Front Immunol 2022;13:1011943.
61. Hao NB, Lu MH, Fan YH, Cao YL, Zhang ZR, Yang SM. Macrophages in tumor microenvironments and the progression of tumors. Clin Dev Immunol 2012; 2012:948098.